Influence of Blade Deformation on Integral Characteristic of Axial Flow Fan

Matjaž Eberlinc*,[1] - Matevž Dular[1] - Brane Širok[1] - Bojan Lapanja[2]
[1]University of Ljubljana, Faculty of Mechanical Engineering, Slovenia
[2]Hidria Institute Klima, Godovič, Slovenia

Axial flow fan blades deform during operation due to the various forces that act on them. That is why, we can ask ourselves about the influence of the blade deformation on the integral and local characteristics. In the paper, we present a study of influence of axial flow fan blade deformation. The paper deals with measurements of the blade deformation at the known integral working conditions. Results - deformations of fan blade tip were used for numerical study of the influence of the changed blade form on the fan's aerodynamic characteristic. Fan integral characteristics were measured in accordance with the ISO-DIS 5801:2006 standard and were carried out on the wind tunnel of the Hidria Institute Klima, Godovič. Other measurements of the blade deformation were done on the measuring station on the Faculty of Mechanical Engineering, University of Ljubljana, with the help of computer aided visualization. Deformations were measured in three working points, which were defined with fan integral parameters.

Results of the measurements helped to determine modified form of the blade, which was then used for the numerical simulation for the same fan integral parameters. The study of deformation influence, based on the numerical simulation, was carried out.
Keywords: axial flow fan, blade deformation, visualization

0 INTRODUCTION

With the development of fans, more often numerical supported CFD methods are used, which can enable predictions of machine's integral characteristic and local flow properties. Method used here is based on the exact defined geometry of the flow tract, which was given on the basic precedent selection and boundary conditions, which were set on the machines basic nominal properties. Blade geometry of the rotor, which presents the essential element of the flow tract is constant and during simulation is not treated as deformation body. In real working conditions on the axial flow fan blade and axial flow pump blade, distinctive transformation can appear, which mainly reflects the changes of the profile angle on the tip position of the blade. This feature can typically influence the machine's actual characteristic. Because deformations are generally not considered in CFD analysis, there poses a question of the assessment of the deformation influence on the integral and local level of the analysis.
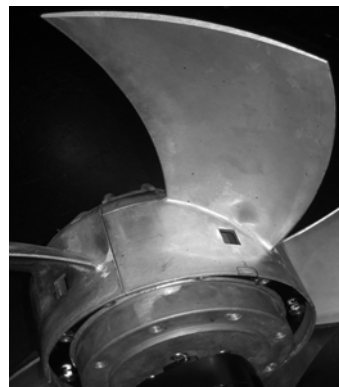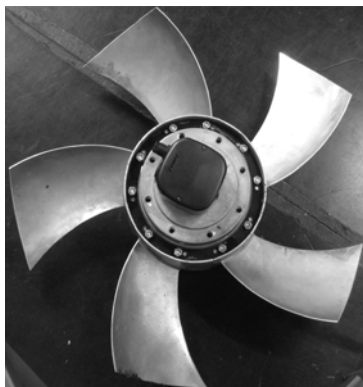
Fig. 1. *Axial flow fan ⌀630 mm with five profiled blades* [1]

*Corr. Author's Address: University of Ljubljana, Faculty of Mechanical Engineering, Aškerčeva 6, SI-1000 Ljubljana, Slovenia, matjaz.eberlinc@fs.uni-lj.si

As an example we present in this paper the influence of blade deformation on the integral and local characteristic of axial flow fan ∅630 mm with five profiled blades, which is shown in Figure 1 [1].

Blade is effected by centrifugal and pressure force while working in steady working point. Centrifugal force occurs in reaction to a centripetal acceleration, acting on a mass and is equal in magnitude to the centripetal force, directed away from the center of rotation (Fig. 2), pressure force is a result of flow conditions in flow cross section of the rotor axial cascade. Resultant of the pressure forces is divided into axial and circumferential component. Axial force is estimated on the basis of pressure difference in and out of the fan rotor and is a result of the working point. On the other hand, circumferential component is estimated with moment on fans axle [2]. Nevertheless, it has to be pointed out that the integral analysis mentioned above, does not give the handling of resultant pressure force, which prevents from estimating load state on the points of blade fastening. In such a manner, we have to take into account that fan blades are exposed due to pressure fluctuations, as a consequence of turbulent flow. Pressure disturbances are a distinctive generator of blade oscillation around its poise position.

The aim of this paper is to determine the influence of deformation on axial flow fan integral characteristic. On the other hand, when we are looking from local prospective, this paper is mainly directed to determine changes of flow properties and static pressure distributions on the blade surface

as a consequence of blade geometry change during operation. Fig. 3 presents procedure of determining the influence of blade deformation on axial flow fan aerodynamic characteristic. Measurements were divided into three stages. In the first stage, measurements of axial flow fan integral characteristic, carried out at the Hidria Institute Klima, Godovič are presented. The purpose of these measurements is mainly, to determine fan's optimum working point. Selection of fan's working points was made, where in continuation of the study, deformation measurements and numerical CFD simulation of fan's aerodynamic characteristics were carried out [5] to [7].

In the second stage, in the selected working point, blade deformation measurements on the measuring station on the Faculty of Mechanical Engineering, University of Ljubljana, were carried out. Computer aided visualization was used, to determine the deformation of fan blades tip [3]. Analysis mainly aimed to estimate absolute deviation of measuring points in meridian surface of flow field, which enabled to detect deformations of blade tip, regarding reference point, located on

Fig. 2. *Deformations, due to axial and centrifugal forces*
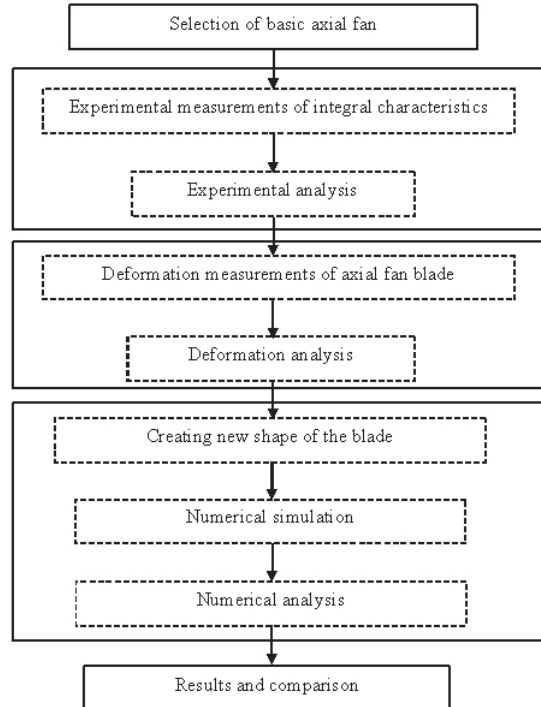
Fig. 3. *Procedure for determining the influence of blade deformation on axial flow fan integral characteristic*

Eberlinc M. - Dular M. - Širok B. - Lapanja B.

the fan casing. Data obtained, subsequently enabled the statistic assessments of deformation conditions on the observed blade. Assessment of oscillating amplitude depends on maximum standard deviations of time-averaged deviation. On the secondary axis the corresponding standardized visualization of time averaged blade deformation and fluctuations of blade tip around its poise position enabled evaluation of blade geometry changes on the field, which is of highest importance for fan operation.

1 INTEGRAL CHARACTERISTIC MEASURMENTS

Measurements were performed at the equivalent working conditions and equivalent working points, to achieve the desired comparisons with the results. Figure 4 shows the integral characteristic of axial flow fan ∅630 mm with five profiled blades, which was measured at the Hidria Institute Klima, Godovič [1]. Point A in Figure 4, at which deformation measurements were carried out, is given in the diagram. In point A, a difference in static pressure Δp_s was defined, which was used to determine the reference parameter in wind tunnel (Fig. 5). Pressure difference was measured with differential pressure transmitter Endress + Hauser Deltabar S PMD75, with measuring uncertainty of 0,05 %.

2 MEASUREMENTS AND ANALYSIS OF DEFORMATIONS WITH COMPUTER AIDED VISUALIZATION

In the Laboratory for water and turbine machines at the Faculty of Mechanical Engineering, University of Ljubljana, deformations with computer aided visualization were measured [2]. Experiment was carried out on the measuring station, which is shown in Fig. 5. Measurements were performed in accordance with recommendations written in standard ISO 5151:1994 [8]. Working conditions were set with integral parameters:
- axial flow fan motor rotations per minute: $n = 1344$ rpm,
- fan static pressure difference: $\Delta p_s = 241$ Pa,
- air density: $\rho = 1.15$ kg/m^3.

Fan static pressure difference and rotor rotating velocity were measured. On the basis of this data it was possible to set the desired fan working point. Camera Dragonly Express IEEE-1394 with objective Pentax Precision Co. B25140, 25 mm was used for image capturing. The camera was triggered with inductive sensor, which was in front of fan rotor. Triggering enabled to set the desired repetition of the blade's location, when the blade was crossing by the hole on the fans casing, regarding the selected reference point, which is also located on the fans casing – point T_0 on Figure 6 a).
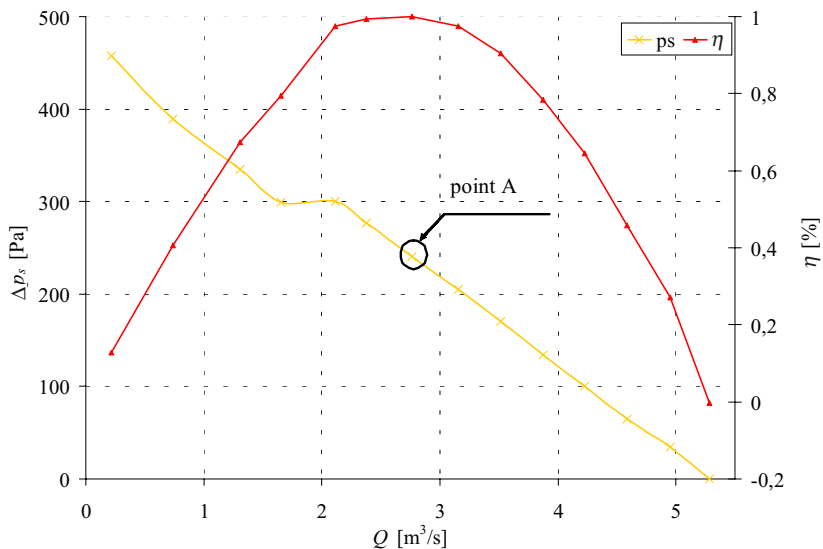
Fig. 4. *Axial flow fan integral characteristic* [1]
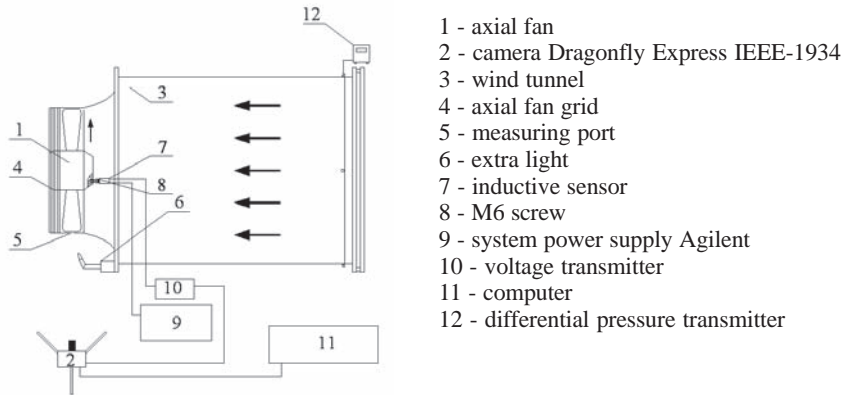
1 - axial fan
2 - camera Dragonfly Express IEEE-1934
3 - wind tunnel
4 - axial fan grid
5 - measuring port
6 - extra light
7 - inductive sensor
8 - M6 screw
9 - system power supply Agilent
10 - voltage transmitter
11 - computer
12 - differential pressure transmitter

Fig. 5. *Measuring station scheme of axial flow fan blade deformation measurement*

Digital images were made with triggering of the camera in the selected time period, which belong to the chosen blade position. Software package LabView was used for controlled capturing of digital images. Images were processed with the help of Matlab software package. For every discussed example, 150 successive images were used, which is satisfactory for statistic estimation – time averaged blade deformation and appurtenant standard deviation of fluctuation around mean value.

Three measuring points (T_1, T_2 in T_3) on the blade tip were selected, enabling the estimation of rotating deviations of the selected measuring points, with respect to reference point T_0 (Fig. 6 a).

Figure 6 b presents the relation between the reference point T_0 on the fan casing and measuring points T_1, T_2 and T_3 on the blade tip. Starting point of Cartesian coordinate system (Fig. 6 b) was reference point T_0. Measuring points on the blade tip T_i (i = 1, 2, 3) were, regarding the selected coordinate system, given by coordinates x_i and y_i.

Measurement uncertainty is mainly accumulated due to assessment of influence on high-speed camera time deviation, while triggering and capturing digital images of the blade. Plain estimation of measurement uncertainty is while determining selected fan working points, which is conditioned mainly with determining the rotating velocity and is accordance with ISO/WD 5801

(a)   (b)
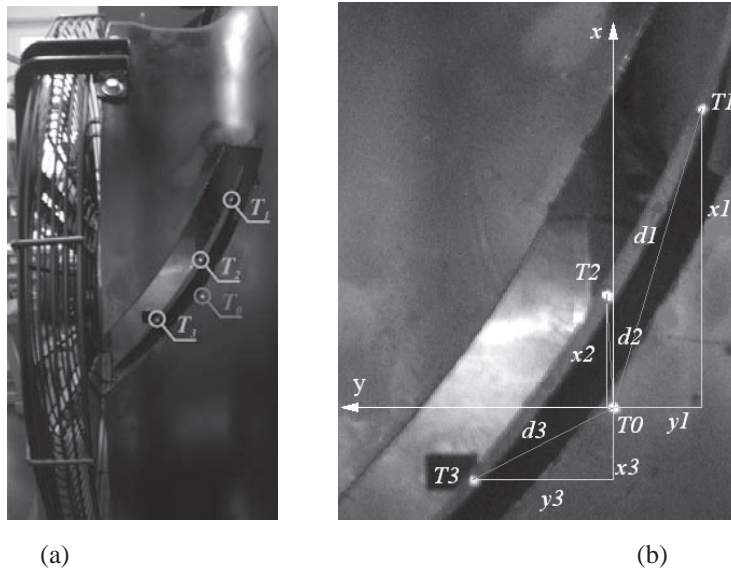
Fig. 6. a) *Axial flow fan blade measuring position;* b) *Scheme presentation of selecting the points for analysis, made by software package AutoCad*

standard estimated with u_n = 0,2 %, measuring pressure difference on the fan u_p = 1,4 % and determining air density in flow, which is, if every procedure is in accordance with the standard, equal to u_ρ = 0,4 %. Measurement uncertainty of visualization method of blade deformation measurements can be divided only on the basis of each step of the presented method. It results from circumferential velocity of the blade tip, fans rotor diameter and frequency of capturing the inductive sensor signals, which triggered digital camera. The highest possible absolute measurement uncertainty is 0.038°, which does not, at the expected maximum blade deformations be approximately 3°, exceed the relative measurement uncertainty of u_v = 1,3 %.

Algorithms for recognizing the digital image samples – measuring points and calculation of measuring points position were elaborated in software package MatLab. Algorithm was aimed to recognize single measuring point on the blade tip and in continuation determining center of a measuring point, which gave the momentarily measuring point coordinate, regarding the starting – reference point T_0. Considering the fact that digitalization was carried out by 8-bit divisibility, where the value of the variable $E_p(i,j,t)$ in Eq. (1), which represents the value of the grey intensity (i, j) in period of time t, is in range:

$$E_p(i, j, t) \in \{0, ..., 255\} \qquad (1).$$

Indices i and j of element E digital image, present the position of the cell. In observed field in formed cell – size of the window (di, dj), where di in dj presents the size of the window.

For every separate image in the sequence of blade tip digital image, scalar value function $f(i,j)$ was calculated, obtained by:

$$f(i, j) = \frac{1}{di} \frac{1}{dj} \sum_{i_p=1}^{di} \sum_{j_p=1}^{dj} E_p\left(i_c + i_p, j_c + j_p\right) \quad (2),$$

where i_c and j_c are coordinates of the selected window. Value of grey intensity E_p in point (i,j) has boundary values from 0 (black colour) to 255 (white colour). In the observed area the function $f(i,j)$ is changed significantly from crossing black field to white field, which belongs to each measuring point T_0, T_1, T_2 and T_3.

To set the edges of measuring points, gradient value of $f(i,j)$ is calculated in the next step,

where maximum scalar value allows determining of the edge of measuring point. Procedure of determining the contour of measuring point is the same in all observed measuring points T_1, T_2 in T_3 and reference point T_0. In the final stage, center of a contour for the selected measuring T_1, T_2 in T_3 and reference point T_0 is calculated.

Position, as well as distance between measuring points on the blade tip and reference point T_0 on the fan casing are time-varying. From the analysis of time successive digital images, the evaluation of fluctuation deviation of measuring points can be carried out, which enables the assessment of average deformation of tip position and assessment of fluctuation intensity of momentary deviations of observed measuring points regarding the time-averaged deformation image.

In this paper, on the basis of presented algorithms, blade tip main deviation values and standard deviation regarding the main deformation values, which are presented in the following chapter, were calculated.

3 EXPERIMENTAL RESULTS

At working conditions, given with point A in fan integral characteristic, shown in Figure 4, sequences of digital images were saved. Figure 7 shows the qualitative comparison of fan rotor at standstill (n = 0 rpm) and at the known rotating
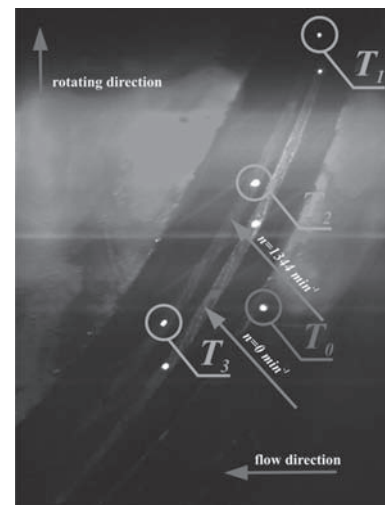
Fig. 7. *Comparison of position of the axial flow fan blade in two working points*
(n = 0 and 1344 rpm)

velocity (n = 1344 rpm) in working point A (Fig. 4). For easier demonstration of the blade deviation, the blade image in two different working points was joint with the help of software package MatLab into one image, shown in Fig. 7. Blade deviation along the blade tip is clearly seen. Distinctive blade deformation is visible, which is reflected in deviation, as well as blade tip distortion.

Quantitative analysis is based on methodology of determining the position of measuring points regarding the reference point T_0, as it was presented in chapter 1. In first stage the length between measuring and reference point was set. Length between points T_1, T_2, T_3 and point T_0 was calculated in two working points of the fan (n = 0 and 1344 rpm), as presented in Figure 6. Time-averaged deviation and standard deviation is given in standard form:

$$x^* = \frac{x}{R_o} \cdot 100\%, \quad y^* = \frac{y}{R_o} \cdot 100\%, \quad d^* = \frac{d}{R_o} \cdot 100\%$$

$$\sigma_x^* = \frac{\sigma_x}{R_o} \cdot 100\%, \quad \sigma_y^* = \frac{\sigma_y}{R_o} \cdot 100\%, \quad \sigma_d^* = \frac{\sigma_d}{R_o} \cdot 100\% \tag{3}$$

where R_0 is fan radius.

In Figure 8 standardized deviations of measuring points on axial flow fan blade tip are presented. On the basic axis time-averaged deviation x^*, y^* in d^* for measuring points T_1, T_2 and T_3 are given. On the secondary axis the corresponding standardized standard deviations $\sigma_x^*, \sigma_y^*, \sigma_d^*$ are given.

Similar deviations in all directions of coordinate system were perceived with the fan – Figure 6 b). In the direction of x axis, deviation of

blades tip towards the outlet of flow is perceived. On the inlet edge of the blade tip smaller deviation are seen, similar as on the outlet edge of the blade tip. This occurrence influences on the change of blade angle of attack and indirectly on the fan integral characteristic. In the direction of y axis (Fig. 6b), deviations are minimal, which is the result of blade shape. Collective deviation is combined from deviations of above-mentioned directions, shown in Figure 8.

4 NUMERICAL SIMULATION OF THE FLOW

Fluid flow through the fan was treated in a steady condition. Simulations in five working points were done. In one series of simulations, blade deformation was considered; in other series it was not (determining blade deformation geometry is presented in 4.1). Software package Fluent 6.1.22 was used, where system of Reynolds average Navier-Stokes equations were computed. Mass conservation equation (Eq. 4) and momentum conservation equation (Eq. 5) along with equations of k-ω SST turbulence model (Eq. 6 and 7) are forming a closed system of equations [4]:

$$\frac{\partial \rho}{\partial t} + \frac{\partial (\rho \bar{u}_j)}{x_j} = 0 \tag{4}$$

$$\frac{\partial (\rho \bar{u}_i)}{\partial t} + \frac{\partial (\rho \bar{u}_j \bar{u}_i)}{\partial x_j} =$$

$$= -\frac{\partial \bar{p}}{\partial x_i} + \frac{\partial}{\partial x_j} \left[\mu \left(\frac{\partial \bar{u}_i}{\partial x_j} + \frac{\partial \bar{u}_j}{\partial x_i} \right) - \rho \overline{u_i' u_j'} \right] \tag{5}$$
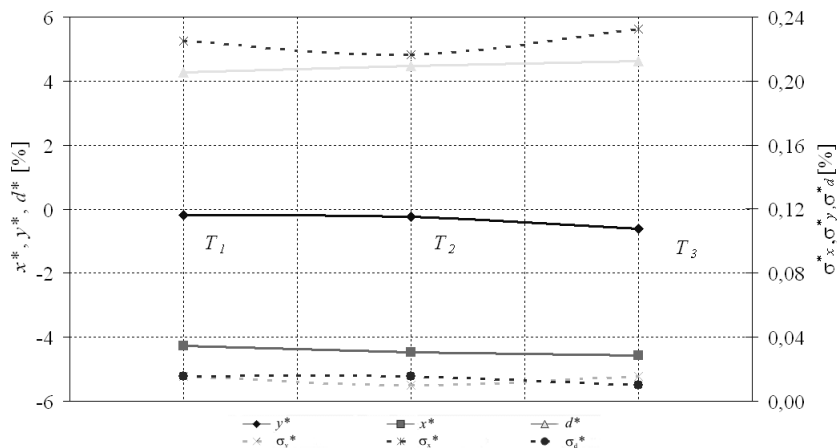
Fig. 8. *Deviation and standard deviation for three measuring points in two working points (n = 0 and 1344 rpm)*

$$\frac{\partial(\rho k)}{\partial t}+\frac{\partial(\rho k \overline{u}_j)}{\partial x_j}=\frac{\partial}{\partial x_j}\left[\Gamma_k \frac{\partial k}{\partial x_j}\right]+\tilde{G}_k - Y_k \quad (6),$$

$$\frac{\partial(\rho \omega)}{\partial t}+\frac{\partial(\rho \omega \overline{u}_i)}{\partial x_j}=\frac{\partial}{\partial x_j}\left[\Gamma_\omega \frac{\partial \omega}{\partial x_j}\right]+G_\omega - Y_\omega + D_\omega \,(7),$$

where $\tilde{G}_k$ is the turbulence source, due to of velocity gradient, G_ω is the source of ω. Γ_k and Γ_ω are the effective diffusivity k and ω. Y_k and Y_ω are dissipations of k and ω, due to of turbulence, D_ω is the diffusive term.

4.1 Geometry and Mesh

With measurements (chapter 3) the blade deformation of blade tip was determined. To be able to set the deformed blade geometry, following procedure was adopted:
- that blades (at fixing area on the motor) are not deforming,
- deformations are increasing linearly from the root to the tip of the blade,
- blade deformation in fans different working points does not significantly change.

Comparison between blade original and deformed geometry is shown in Figure 9.

Meshes of original and deformed blade were topologically equivalent. Computational domain was discretized with structural mesh. To reduce the calculating time, only one interblade area (1/5 total area) was calculated, on borders a periodic boundary condition was regulated. Influence of the mesh was examined only at optimum flow and for the case of original – not deformed blade. Finally, the mesh with approximately 400.000 nodes was used, which was on the channel walls and along

■ original blade
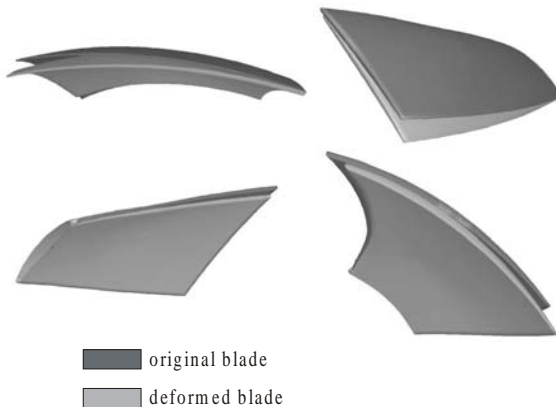
▨ deformed blade

Fig. 9. *View of original and deformed blade*

the fan blade refined - y^+ was between 30 and 80. With this kind of mesh density we evaluated the error of discretization to 0,5 %. Geometry, as well as deformed blade mesh, was equivalent for all working points - it was adopted, that for every single working point of the axial flow fan, deformation does not change significantly.

4.2 Convergence Criterion

Convergence criterion was set, regarding the pressure development on the inlet and velocity on the outlet from the computational domain. Parameters were always converging, when the residuals sum of transport equation in the entire computational domain was less then 1×10^{-3}. Finally, for convergence criterion, the situation was used, when the residuals decreased below 1×10^{-4}, for which approximately 350 iterations were needed. Iteration error was estimated to 0,05 %.

4.3 Calculating Condition

- Flow: for turbulence k-ω SST turbulence model was used;
- Boundary conditions: on the channel walls, fan blade and rotor no slip boundary condition was assumed;
- On the inlet air flow was defined ($\cong$ 1.31, 2.11, 2.76, 3.52, 4.22 m³/s);
- On the outlet pressure was defined (0.1013 MPa);
- Fan rotating velocity was constant (1344 rpm), fan rotating was described by rotating reference frame model.

Air density was 1.225 kg/m³, dynamic viscosity was 1.79×10^{-5} Pas. The results from numerical simulation are presented in chapter 5.

5 RESULTS

Results from prediction of flow fields for original and deformed – modified form of the blade in various working points of the machine, final numerical predictions and axial flow fan integral characteristic measurements are presented.

5.1 Numerically Predicted Blade Pressure Distribution

Pressure distributions in three different working points of the fan (1.31, 2.76, 4.22 m³/s)

Original blade   Deformed blade

Pressure side   Suction side   Pressure side   Suction side

$Q = 1.31$ m³/s

$Q = 2.76$ m³/s

$Q = 4.22$ m³/s

5.00e+02
4.15e+02
3.30e+02
2.45e+02
1.60e+02
7.50e+01
-1.00e+01
-9.50e+01
-1.80e+02
-2.65e+02
-3.50e+02
-4.35e+02
-5.20e+02
-6.05e+02
-6.90e+02
-7.75e+02
-8.60e+02
-9.45e+02
-1.03e+03
-1.12e+03
-1.20e+03
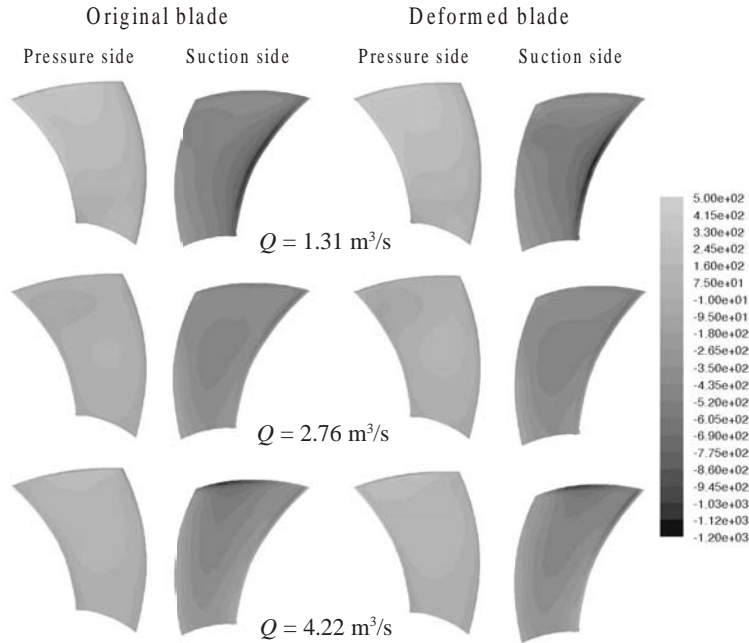
Fig. 10. *Pressure distribution for original blade geometry and deformed blade geometry*

Original blade   Deformed blade

Pressure side   Suction side   Pressure side   Suction side

$Q = 1.31$ m³/s

$Q = 2.76$ m³/s

$Q = 4.22$ m³/s
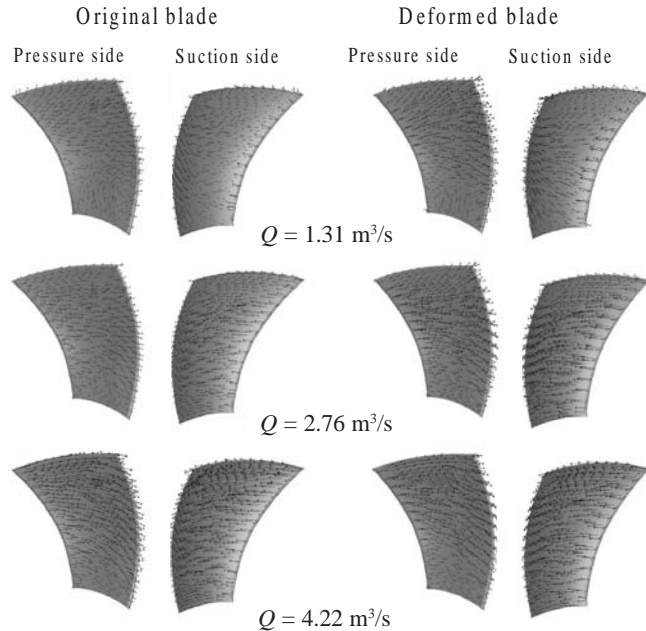
Fig. 11. *Relative velocity vectors on pressure and suction side of original and deformed blade for fan three working points*

are presented in Figure 10. Presented pressure distributions on the pressure and suction side for case of original blade geometry (left) and for case of deformed blade geometry (right).

Pressure distribution on blade is similar for both, the original and deformed blade. At lower flow

($Q = 1.31$ m³/s) it can be noticed, that pressure on suction side of the deformed blade is slightly lower, which effects the intensive separation of flow at this location. The reason for this is a larger blade angle of attack, because of deformation. Near the optimum ($Q = 2.76$ m³/s) changes are less distinctive, pressure

on suction side of deformed blade is slightly lower that in the case of original blade. In working point 4.22 m³/s, pressure conditions on blade are not distinctive. Pressure on the trailing edge on the section side of the deformed blade is slightly higher in comparison to the pressure on the same place of the original blade. The difference is the result of better flow conditions for the deformed blade, because the angle of attack is larger (optimum moves to the higher volume flow).

Despite the deformations, conditions on the blade pressure side remain mostly the same, and changes are negligible.

5.2 Numerically Predicted Velocity on the Blade

Figure 11 shows relative velocity vector on pressure and suction side of original and deformed blade in fan's three different working points ($Q = 1.31, 2.76, 4.22$ m³/s).

It can be noticed, that in case of smaller volume flow ($Q = 1.31$ m³/s), the flow on the deformed blade is less settled. On the blade tip on suction side, a large vortex can be seen, which is smaller in case of original blade. The cause for

detaching of flow on this side and this working point is a larger angle of attack of the blade, which is even larger, because of deformation. We can also see a larger disorder of flow on the pressure side of the deformed blade. It seems that vectors point from the middle side of the blade in direction towards the tip and root of the blade. The reason is that flow cannot follow increased curvature of blade and hits into it, instead of flowing around it.

Near the optimum point ($Q = 2.76$ m³/s) the differences in flow field are less distinctive. On the suction side of the deformed blade, on the top, near the trailing edge, a field of lower velocity is seen, which can be assigned to separating of flow on this place (the reason again being larger blade angle of attack). Similar (but less obvious) as in the case of a smaller volume flow, hitting of the flow against the pressure side of the deformed blade can be seen.

At higher volume rate ($Q = 4.22$ m³/s) differences are not visible.

5.3 Velocity on Blade Tip

In Figure 12 relative velocity vectors are shown on the section 15 mm from the tip of the

Original blade　　　　　Deformed blade

$Q = 1.31$ m³/s

$Q = 2.76$ m³/s
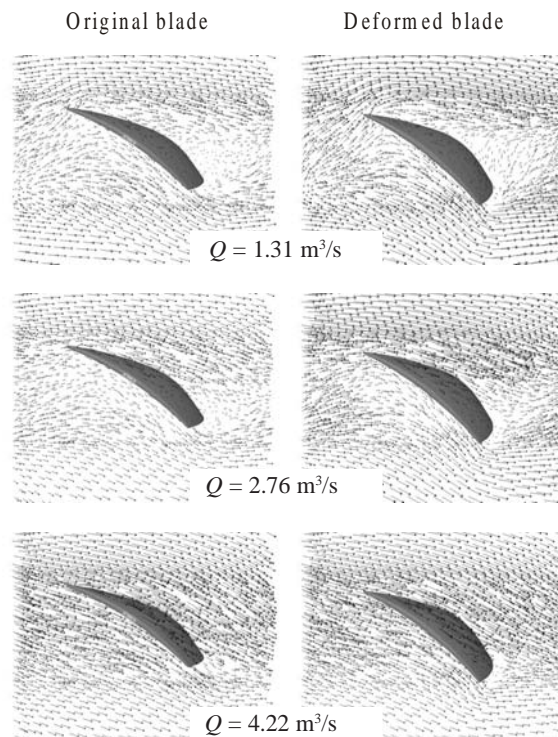
$Q = 4.22$ m³/s

Fig. 12. *Relative velocity vector on the section 15 mm from the tip of the original and deformed blade in fan's three working points*

original and deformed blade in fan's three working points (Q = 1.31, 2.76, 4.22 m³/s).

Images show velocity conditions at the most critical place (at the tip of the blade). Separating of flow on this place causes the efficiency and power drop and generation of aerodynamic noise.

At the lower and optimal flow (Q = 2.76 m³/s) the separating of flow is obviously larger in case of deformed blade, which is the result of inappropriate (larger) blade angle of attack. In case of higher volume flow (Q = 4.22 m³/s) the aggressiveness of separating between the blades is comparable, which is the result of shifting the optimum towards higher volume flow, because of blade deformation.

5.4 Predictions and Measurements of Integral Characteristics

Figure 13 shows measured and numerical (for original and deformed geometry) integral characteristic of standardized efficiency and pressure increase in dependence of volume flow.

Numerical model with original blade geometry agrees with measurement results near the optimum working point, otherwise deviations are higher. It is different with the results obtained from numerical model with the deformed blade geometry, which match with experimental results in wider range. Higher deviation can be seen at lower volume flow, which is probably the result of overestimated prediction of flow separation of trailing edge of the blade and incorrect estimation of blade deformation (for every case, measured deformation in optimum working point was considered – in chapter 3).

Suitableness consideration of actual (deformed) shape of the blade is obvious, because there is an option for better prediction of actual flow field and easier optimization of blade geometry.

6 CONCLUSION

This paper presented the influence of blade deformation on fan integral and local characteristic. With computer aided visualization blade tip deformations were defined. Measurement results were used to determine the variable blade formation, which was in continuation used for numerical modeling for the same fan integral working parameters. Considering to use actual (deformed) shape of the blade would be suitable in this case, because it enables better prediction of actual flow field and easier optimization of blade geometry.
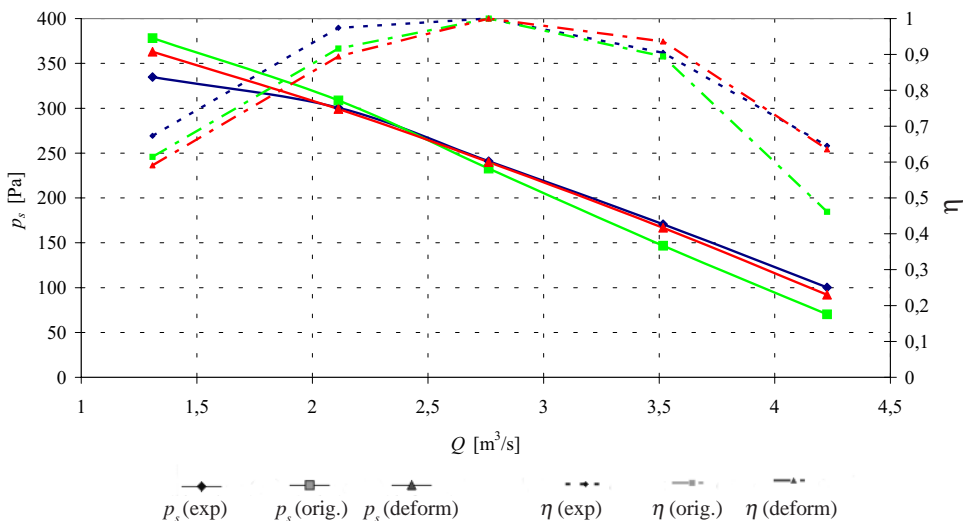
Fig. 13. *Comparison between the experimental results and numerical model for cases of original and deformed geometry*

cooling; Research of elements of power saving and environmental friendly CHC systems.

7 REFERENCES

[1] Pivk, S., Magajne, A., Tominec, U. *Measurements of integral properties of axial flow fan with 630 mm radius*. Sp. Idrija: Hidria Rotomatika, d.o.o., July 2006. (In Slovenian).

[2] Wallis, R. A. *Axial flow fans and ducts*. John Wiley & sons, 1983.

[3] Eberlinc, M., Hočevar, M., Pivk, S., Širok, B. Visualization method for measuring the deformation of axial-flow fan blades, *Ventil*, 13, 2007, no. 2, p. 94-101.

[4] Ferziger, J.H., Perić, M. *Computational Methods for Fluid Dynamics*, 3rd Edition. Springer, 2002

[5] Širok, B., Bajcar, T., Dular, M. Reverse flow phenomenon in a rotating diffuser. *J. flow vis. image process*, 2002, vol. 9, no. 2/3, p. 193-210.

[6] Širok, B., Hočevar, M., Zupan, S., Prebil, I. Study of radial rotor and bearing arrangement dynamic properties of the combat vehicles M 84 and 72 cooling system fan. *Stroj. vestn. - J. Mech. E.*, 1999, vol. 45, no. 11, p. 432-441.

[7] Širok, B., Potočar, E., Novak, M. Analysis of the flow kinematics behind a pulsating adaptive airfoil using computer-aided visualisation. *Stroj. vestn. - J. Mech. E.*, 2000, vol. 46, no. 6, p. 330-341.

[8] ISO 5151:1994: *Non-ducted air conditioners and heat pumps - Testing and rating for performance*

[9] ISO 5801:2006: *Industrial fans*